ChemPubSoc Europe

DOI: 10.1002/chem.201702586

CHEMISTRY A European Journal Communication

Metal–Organic Frameworks

Assessing Guest-Molecule Diffusion in Heterogeneous Powder Samples of Metal–Organic Frameworks through Pulsed-Field-Gradient (PFG) NMR Spectroscopy

Roland Thoma,[a] Jörg Kärger,*[b] Nader de Sousa Amadeu,[a] Sandra Nießing,[a] and Christoph Janiak*[a]

Abstract: Investigation of guest diffusion in porous metal–organic frameworks (MOFs) is of major importance, because many porosity-related properties of MOFs are influenced by diffusion effects. The diffusion of dimethyl sulfoxide (DMSO) in the MOF MIL-53-NH_2(Al) was investigated through pulsed-field-gradient (PFG) NMR spectroscopy. The microporous material was synthesized in small crystallites (under 500 nm), which agglomerated in a large range of particle sizes (from hundreds of nanometers to tens of micrometers), giving a morphologically very heterogeneous sample. No special agglomeration pattern could be observed, which makes a PFG NMR investigation very challenging, yet it represents a realistic situation for the diffusion of guest molecules in porous materials. We were able to distinguish between two diffusion regimes existing in parallel with each other over the total range from 15 to 200 ms of observation times as accessible in the experiments: In the large crystal agglomerates (diameters above 20 μm), guest movement was found to be subdiffusive, with a time exponent $\kappa = 0.8$ (rather than one as for normal diffusion). Guest diffusion in the remaining, smaller host particles followed the pattern of normal diffusion within a bed of spheres of impenetrable external surfaces, with a size distribution in good agreement with that of the material under study. Diffusion in a rather complex system could thus be referred to a two-region model with new potentials for application to systems of intricate topology.

In general, guest diffusion inside porous host media is influenced by many parameters, such as pore size, adsorbing inner surfaces, pore/channel geometry (as well as their connectivity), and host–guest interactions to name but a few.[1,2] Due to the texture of most porous materials, the measurement of guest diffusion has become a sophisticated task. Beside microscopy methods[2,3] and quasi-elastic neutron scattering (QENS),[4,5] pulsed-field gradient (PFG) NMR technique appeared to be a suitable method for observing molecular diffusion in microporous materials (see the Supporting Information for a brief treatise on the theory of PFG NMR and diffusion).[1,6,7] The investigation of guest diffusion through PFG NMR is notably facilitated when the host material has a known and well-ordered structure, such as narrow particle size distribution, homogenous and large host particle sizes or an easy-to-infer diffusivity inside particles.[1,2] Thus, much effort has been made to study such idealized systems.[8–11] It is true that recent progress in PFG NMR methodology[12] has facilitated diffusion studies in also more complex pore architectures[13–16] just as the investigation of highly heterogeneous systems being characterized by a distribution of diffusivities.[16,17] However, application of such advanced techniques requires high accuracy in the spin-echo attenuations, which cannot be expected to be attainable as a rule. Herein, we used the functionalized MOF MIL-53-NH_2(Al)[18] (see Figure S1 in the Supporting Information for the structure), which has shown very interesting properties in gas, especially, CO_2 adsorption,[18–21] photophysics,[22,23] and catalysis.[23,24] Primary particles of MIL-53-NH_2(Al) show a tendency for agglomeration (Figure S5 a–u in the Supporting Information), which depends on the synthesis conditions.[25,26] In contrast to MIL-53-NH_2(Al) monocrystals, agglomerated materials can show higher Brunauer–Emmett–Teller (BET) surface areas and micropore volumes.[25] Experience shows that MOF synthesis very often gives samples with not very well-shaped crystallites, also of different shapes and a wide size distribution and with agglomerated primary particles.

This fact can render MOF materials far from ideal for model studies, yet the material can have the sought-after properties and be of technological relevance. The diffusion behavior of guest molecules in such more realistic systems is still poorly investigated. This work presents a new approach to understand the diffusion phenomenon on the time scale of PFG NMR spectroscopy (ms to s) and provides the first PFG NMR investigation on MIL-53-NH_2(Al). The usage of DMSO as a guest mole-

[a] R. Thoma, Dr. N. de Sousa Amadeu, S. Nießing, Prof. Dr. C. Janiak
Institut für Anorganische Chemie und Strukturchemie
Heinrich-Heine-Universität, 40204 Düsseldorf (Germany)
E-mail: janiak@hhu.de

[b] Prof. Dr. J. Kärger
Department of Interface Physics
Leipzig University, Linnéstrasse 5, 04103 Leipzig (Germany)
E-mail: kaerger@physik.uni-leipzig.de

Supporting information and the ORCID identification number(s) for the author(s) of this article can be found under: https://doi.org/10.1002/chem.201702586. It includes characterization of the sample MIL-53-NH2(Al) by powder X-ray diffraction (Figure S3 a–d), nitrogen-porosity measurements (Figure S4 a, b), and scanning electron microscopy (Figure S5a–u).

cule is based on its physical and chemical properties. Because the scope of this study is focused on probing the agglomerated crystallites in terms of their inter- and intra-particle porosity, we needed: 1) a low diffusivity of the tracer molecules; 2) a neglectable vapor pressure; 3) a micropore accessible molecular volume; 4) a melting point between 10 to 20 °C (ensuring straightforward freezing upon moderate cooling). Further, the sorption of DMSO does not change the MIL-53 structure, as was evidenced by the identical powder X-ray diffractogram in the DMSO-free and DMSO-loaded state (Figure S3 d in the Supporting Information), that is, DMSO does not induce a breathing effect,[19] that is, a transition from the empty, activated large-pore to the narrow-pore form. To better understand the MOF aggregation behavior, we have analyzed the particle-size distribution from scanning electron microscopy images (Figure 1 (top) and Figure S5a–u in the Supporting Information). The resulting agglomerate diameter distribution showed a maximum abundancy of approximately 30% for agglomerates of 10 ± 5 μm outer diameter (Figure 1, top).

To estimate the amount of guest molecules inside an agglomerate of specific diameter d, we approximated the volume of each agglomerate by d^3 and the guest molecules density as homogeneous along the inner volume of all agglomerates. The result is shown in Figure 1 (bottom) and was calculated by using Equation (1), with $n(2R_j)$ indicating the number of agglomerates with radii between R_{j-1} and R_j. This approach implies that the major parts of the guest molecules are confined in the few but large agglomerates ($d>60$ μm). On the other hand, small agglomerates ($d<10$ μm) account for the major part of the host particles, but contain only a minor part of the guest molecules (see above).

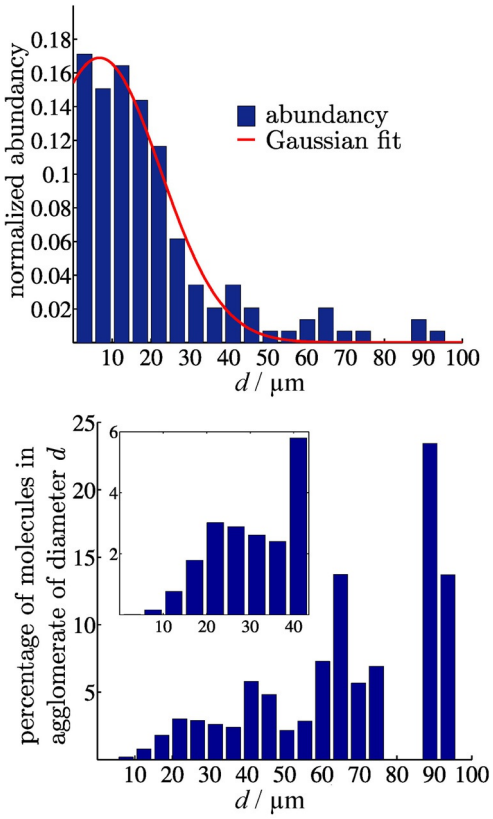

Figure 1. Top: Agglomerate diameter abundancy distribution ($\propto A_j$) with Gaussian fit. This fit gave a mean diameter of 7 μm with a standard deviation σ of 3 μm. Bottom: Percentage of DMSO guest molecules ($\propto P_j$) inside an agglomerate of specific diameter. The inset shows a magnification of the range between 1 μm–40 μm.

$$P_j(V_j) = \frac{A_j(n(2R_j))R_j^3}{\sum_{k=1}^{n} A_k(n(2R_k))R_k^3}$$
$$A_j(n(2R_j)) = \frac{n(2R_j)}{\sum_{k=1}^{n} n(2R_k)} \quad (1)$$

A summary of the PFG NMR spin-echo (PFGSE) attenuation curves $E(q,\Delta)$ as the primary data of our diffusion measurements are provided in Figure S1 in the Supporting Information. Value Δ stands for the observation time, which has been varied from 15 to 200 ms; q (varied from 300 to 30000 m^{-1}) is a measure of the intensity of the field gradient pulses. Its reciprocal value indicates the order of magnitude of guest displacements accessible by the measurement (see the Supporting Information for more details). It turned out that, for the system under study, these dependences were reasonably well represented by an approach of the type [Eq. (2)]:

$$E(q,\mathbf{\Delta}) = P_1\exp(-q^2D_1\mathbf{\Delta}) + P_2\exp(-q^2D_2\mathbf{\Delta})$$
$$= P_1\exp(-q^2MSD_1/6) + P_2\exp(-q^2MSD_2/6) \quad (2)$$

which is recognized [see Eq. (S1) in the Supporting Information] as the superposition of the signals stemming from two separate samples (domains) with relative signal intensities P_1 and P_2 and diffusivities D_1 and D_2. In the second equation, we made use of the Einstein–Smoluchowski relation [Eq. (S2) in the Supporting Information] indicating (as the key feature of "normal diffusion") proportionality between the molecular mean square displacement (MSD) and the observation time (with sixtimes the diffusivity appearing as a factor of proportionality). Figure 2 shows the value of the mean square displacements (MSD_j), and the relative signal intensities (P_j) resulting from the best fit of Equation (2) to the experimental data of Figure S1 in the Supporting Information. We note that within the limits of accuracy, as indicated by the error bars in Figure 2 (bottom), the relative signal intensities may be implied to be essentially constant. This holds doubtlessly true up to an observation time of 100 ms, whereas with further increasing observation times, one is confronted with a further, significant decrease in signal intensity by longitudinal nuclear magnetic relaxation, which questions any meaningful quantitative analysis.

We are now going to demonstrate that exactly such dependence may be expected by considering the above characterized two fractions of host particles ("domains") with their guest molecules as giving rise to the two signals. We shall use index 1 (2) with reference to molecules in the small (large) host particles. By doing so, we may easily explain why—deviating from, for example, references [27–29] in which two-range approximations have been introduced and extensively used in

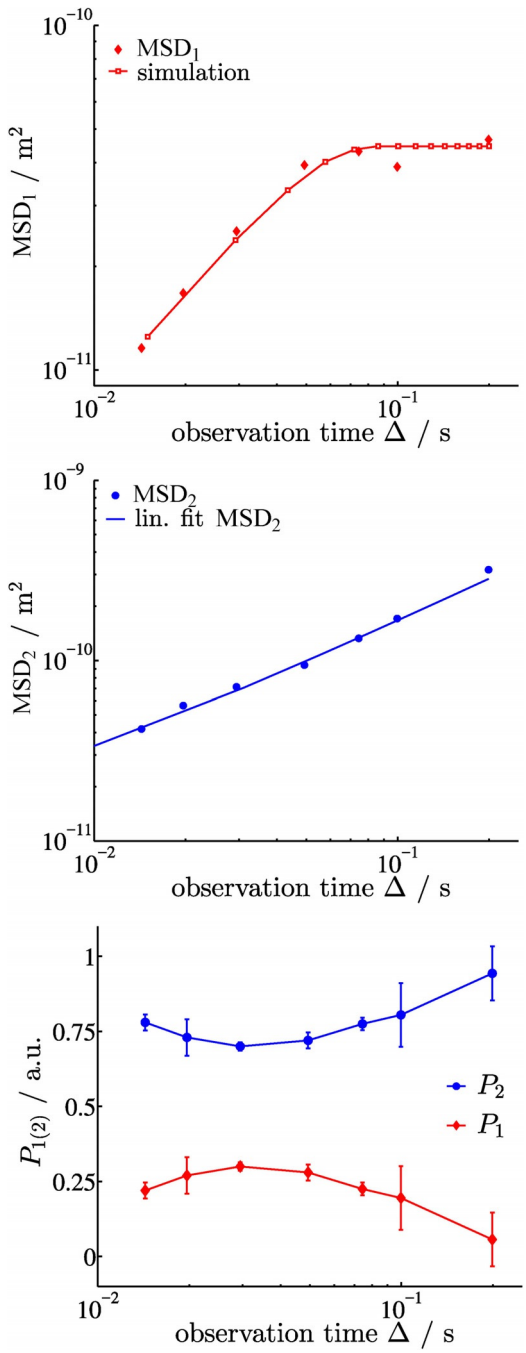

Figure 2. Top: Double logarithmic plot of the mean square displacement of domain 1 (MSD_1) with increasing observation time Δ. The shown curve was simulated as described [Eq. (3)]. Due to the restriction of guest molecules, this plot reveals this domain to be present in the small MOF agglomerates. The plateau corresponds to a RMSD = 7.5 μm (see text for details). Middle: Double logarithmic plot of the mean square displacement of domain 2 (MSD_2) with increasing observation time Δ. The straight line was obtained by a linear fitting procedure according to Equation (S5a) in the Supporting Information. This provides a time exponent $\kappa = 0.8$, which indicates subdiffusive behavior in the large MOF agglomerates (see text for details). Bottom: Semi-logarithmic representation of the probabilities in dependency of the observation times Δ.

PFG-NMR diffusion studies—the relative signal intensities does only scarcely vary with the observation time. This is the consequence of the low gas pressure and the frozen bulk phase, which excludes any notable "intercrystalline" mass transfer and of, second, the fact that the nuclear magnetic relaxation times in both "types" of host particles may be expected to be close to each other. In the following, it shall be demonstrated that the time dependences as appearing from the representations in Figure 2 (top and middle) are in perfect agreement with our model predictions.

Now we would like to discuss diffusion in small agglomerates (domain 1). The plateau observed for domain 1 in Figure 2 (top) corresponds to a confinement space of about 7 μm radius. This behavior could be simulated if we approach the crystal agglomerates shape by spheres of radius R. To describe the time evolution of the diffusion coefficient, we introduced a "matrix" $\widehat{D}_{ij}(\Delta_i, R_j)$ of diffusion coefficients, with the element $\widehat{D}_{ij}$ assigned to diffusion within a sphere of radius R_j during the observation time Δ_i, by making use of the approach [Eq. (3)]:

$$\widehat{D}_{ij}(\Delta_i, R_j) = \begin{cases} D_0 \text{ if } \Delta_i < \dfrac{R_j^2}{5D_0} \\ \dfrac{R_j^2}{5\Delta_i} \text{ if } \Delta_i \geq \dfrac{R_j^2}{5D_0} \end{cases} \quad (3)$$

that is, by considering only the limiting cases of either free diffusion (for times specified in the upper line) or restricted diffusion (lower line). Due to a broad radii distribution, we distinguished two different kinds of agglomerate particles within this domain 1: agglomerates satisfying $\xi < 1$ or $\xi > 1$ [Eq. (S3) in the Supporting Information].

In the former case, guest molecules diffuse unrestricted with a diffusion coefficient $D_0 = \lim_{\Delta \to 0} D(\Delta)$, whereas in the latter case, their effective diffusion coefficient will decrease according to Equation (S4) in the Supporting Information. The time needed for the transition from unrestricted to restricted diffusion can also be estimated by using Equation (S4). We have now to consider that the number of molecules residing in a given particle—and, thus, their contribution to the overall signal, increases in proportion with its volume, that is, with the third power of its diameter. Because we have connected the diffusion coefficient to the agglomerate radii in Equation (3), the varying guest contents correspond to the amount of guest molecules with a certain diffusion coefficient. Based on the knowledge of the particle diameter distribution $A_j(n(2R_j))$ (Figure 1, top), with $d = 2R$, one can describe each volume contribution $P_j(V_j)$, given by the ratio of the abundancy-weighted volume of each agglomerate with a certain radius $A_j(n(2R_j))8R_j^3$ and the total volume of all abundancy-weighted agglomerate volumes $\sum_{k=1}^{n} A_k(n(2R_k))8R_k^3$. This is summarized in Equation (1) and graphically represented in Figure 1 (top). By assuming a loading of 100% and a uniform guest molecule density in each agglomerate, $100\% \times P_j(V_j)$ corresponds to the percentage of guest molecules inside an agglomerate with radius R_j; $P_j(V_j)$ is time independent due to the confinement of guest molecules. Recollecting that $P_j(V_j)$, in this case, corresponds to the abundancy of a certain diffusion coefficient, one can combine Equations (3) and (1) into Equation (4):

$$\widehat{D}_{ij}^{A}(\Delta_i, R_j) = P_j(V_j)\widehat{D}_{ij}(\Delta_i, R_j) \quad (4)$$

This equation gives an abundancy-weighted matrix $\widehat{D}_{ij}^{A}(\Delta_i, R_j)$ of diffusion coefficients, which is graphically represented in Figure 3 (top). As expected, Figure 3 (top) shows that the contribution of each radius to $\widehat{D}_{ij}^{A}(\Delta_i, R_j)$ varies significantly. Although the smallest agglomerate particles contribute only marginal, the agglomerates of approximately 6 μm show the highest contribution. The decrease of $\widehat{D}_{ij}^{A}(\Delta_i, R_j)$ for the largest particle radii is a simple consequence of their vanishing amount and, hence, of the vanishing number of molecules ($\propto P_j(V_j)$) that they are accommodating. At the initial observation times, they form a plateau of unrestricted diffusion and decrease with increasing observation time Δ_i. The medium sized particles ($\approx$3 μm) give significant contributions and the diffusion is restricted at any time Δ_i. Because NMR detects all these contributions simultaneously, the measured diffusion coefficient at every Δ_i is the sum of each column vector along R_j in $\widehat{D}_{ij}^{A}(\Delta_i, R_j)$, as summarized in Equation (5) and Figure 3 (bottom).

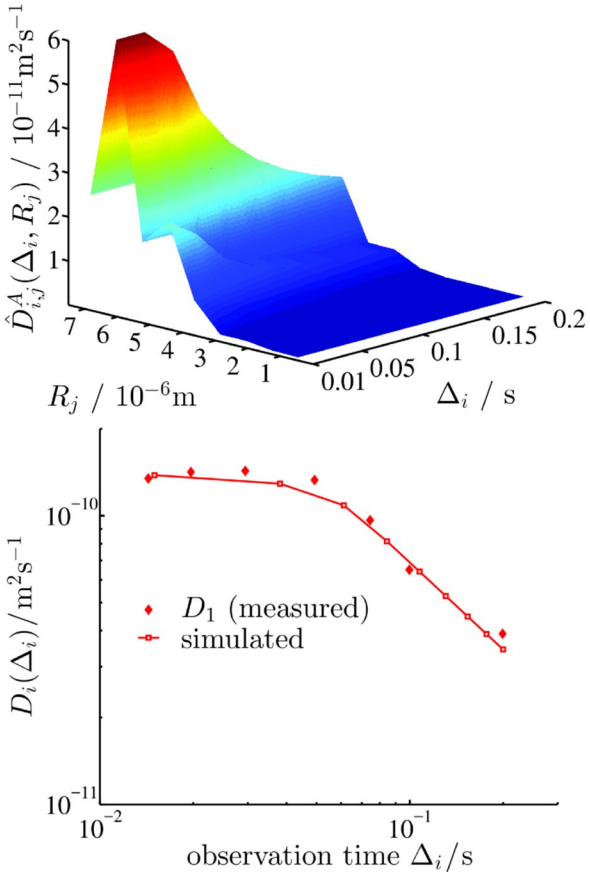

Figure 3. Top: 3D plot of the abundancy-weighted elements of the diffusion matrix $\widehat{D}_{ij}^{A}(\Delta_i, R_j)$ [Eq. (4)] in dependency of the agglomerate radius R_j and observation time Δ_i. Bottom: Comparison of the experimental data D_1 with simulated diffusion coefficients $D_i(\Delta_i)$, which are the weighted sums along each radius-dependent column vector [Eq. (5)]. Figure S7 in the Supporting Information shows a combination of both plots in double logarithmic representation.

$$D_i(\Delta_i) = \sum_{j=1}^{n} \widehat{D}_{ij}^{A}(\Delta_i, R_j) = \sum_{j=1}^{n} P_j(V_j)\widehat{D}_{ij}(\Delta_i, R_j) \quad (5)$$

The corresponding MSD is given by Equation (6), which is simply obtained by insertion of Equation (5) into Equation (S2) in the Supporting Information.

$$\langle R_i^2(\Delta_i)\rangle = 6\sum_{j=1}^{n} \widehat{D}_{ij}^{A}(\Delta_i, R_j)\Delta_i \quad (6)$$

Equation (6) is plotted in Figure 3 (bottom) and shows a significant correlation to the experimentally generated data points. Furthermore, this consideration results in a mean agglomerate radius of 7.5 μm and a $D_0 = 1.42\times10^{-10}$ m^{2}s^{-1}, which corresponds nicely with the experimental data.

Now we would like to discuss the diffusion in large agglomerates (domain 2). Also D_2, the diffusivity in the large particles, has been seen to decrease with increasing observation time, though in a notably more modest way. We know that the echo intensities in PFG NMR data are primarily sensitive to the molecular mean square displacement $\langle R_2^2(\Delta)\rangle$ as a result of Einstein's Equation [Eq. (S2) in the Supporting Information]. The validity of the Einstein equation (i.e., of a time-invariant diffusivity) indicates occurrence of normal diffusion. Any variation of the diffusivity with time may, in turn, be taken as an indication of deviation from ordinary diffusion. By converting the MSD in larger agglomerates, given in Figure 2 (middle), into diffusivities we obtain [Eq. (7)]:

$$D_2 = \frac{\langle R_2^2(\Delta)\rangle}{6\Delta} \propto \Delta^{\kappa-1} \quad (7)$$

with a time exponent $\kappa = 0.8$ (rather than one as required for normal diffusion). As to be expected from first-principle considerations,[1,2,34] mass transfer in regularly structured microporous materials had been found to follow the laws of ordinary diffusion already by the very first PFG NMR diffusion studies with zeolites,[35] which most recently was confirmed by also the direct recording of diffusion fronts by microimaging.[37] Deviations from this pattern—as those expressed by Equation (S2) in the Supporting Information—must therefore be referred to deviations from a regular structure. In particular, this includes the presence of additional transport resistances,[36,38,39] which were shown to correlate with the existence of stacking faults, as was reported by Feldhoff et al.[40] Deviations from normal diffusion with meaningful time exponents over substantial ranges of observation times (and, hence, of displacement) are typical in the presence of spatial hierarchies, such as for spatially correlated distributions of transport resistivity.[2,40,41] The process of agglomeration leading to the particles under investigations is known to potentially give rise to such formations.

The combination of structural analysis with the outcome of diffusion studies thus appears to be a promising topic of continuing research. Because the sizes of the individual crystals were smaller than 500 nm and, thus, notably below the lower limit of measurability of molecular displacement (which, under the chosen conditions, should have been of at least 1 μm), the

channel-like structure of MIL-53-NH_2(Al) is not directly revealed in the PFG NMR diffusion measurements. However, it could be demonstrated that MOF crystal agglomerates with a diameter abundancy distribution can nicely be probed with a slow diffusing guest molecule by monitoring the MSD and time-dependent diffusion coefficient, respectively. Thus, a clear picture of guest diffusion inside the material has been shown to evolve on the basis of already quite elementary assumptions, namely, by dividing the system into two diffusing regimes assigned to small and large agglomerate distributions. Mass transfer in the large agglomerates is found to proceed by anomalous diffusion giving rise to a time exponent $\kappa = 0.8$, which corresponds with a random walker's fractal path dimension (see Equation (S5b) and ref. [2]) $d_\omega = 2.5$, instead of $\kappa = 1$ and $d_\omega = 2$ for normal diffusion.

Thus, the host material itself appears to be a fractal. Interestingly, the highest measured diffusion coefficient of DMSO in regime D_2 of $6.79 \times 10^{-10}\ m^2 s^{-1}$ almost corresponds with the free self-diffusion coefficient of DMSO at 25 °C of $7.31 \times 10^{-10}\ m^2 s^{-1}$.[43] This indicates an expected melting point depression of neat DMSO (T_m(DMSO) = 18.45 °C)[44] of at least ΔT_m(DMSO) = 13.5 °C, because it is inversely proportional to the pore diameter.[45] The diffusion regime D_1 in small agglomerates shows a very different diffusion behavior due to the effect of confinement. The time dependence of the MSD could be simulated by considering the small crystal agglomerates as spheres with radius *R*. This analysis gives a mean diameter of 7.5 μm and a diffusion coefficient $D_0 = 1.42 \times 10^{-10}\ m^2 s^{-1}$.

This value is notably smaller than the short-range diffusivities in the larger particle aggregates, which are thus found to offer diffusion pathways not yet available in the smaller particle. Their specification by refined structural analysis is among the prime challenges of future research work stimulated by the present diffusion studies.

Acknowledgements

We thank Dr. Annika Herbst for help with the SEM images, Mrs. Bahareh Nathegi for help with PXRD measurements and Dr. Markus Rosenstihl (TU Darmstadt) for help with the spectrometer buildup. We are indebted to Prof. Dr. Matthias Karg and Mr. Arne Lerch for help with the DLS measurements and interpretation. The work was supported by the BMBF through grant Optimat 03SF0492C.

Conflict of interest

The authors declare no conflict of interest.

Keywords: anomalous diffusion · metal–organic frameworks · NMR spectroscopy · restricted diffusion

[1] W. Price, *Concepts Magn. Reson.* **1997**, *9*, 299 – 336.
[2] J. Kärger, D. M. Ruthven, D. N. Theodorou, *Diffusion in Nanoporous Materials Vol. 1*, 1st ed., Wiley-VCH, Weinheim, **2012**.
[3] J. Kärger, C. Binder, F. Chmelik, F. Hibbe, H. Krautscheid, R. Krishna, J. Weitkamp, *Nat. Mater.* **2014**, *13*, 333 – 343.
[4] N. J. Rosenbach, H. Jobic, A. Ghoufi, F. Salles, G. Maurin, S. Bourrelly, P. L. Llewellyn, T. Devic, C. Serre, G. Férey, *Angew. Chem. Int. Ed.* **2008**, *47*, 6611 – 6615; *Angew. Chem.* **2008**, *120*, 6713 – 6717.
[5] M. Bée, *Chem. Phys.* **2003**, *292*, 121 – 141.
[6] J. Kärger, H. Pfeifer, W. Heink, *Adv. Magn. Reson.* **1988**, *12*, 2 – 89.
[7] G. Sörland, *Dynamic Pulsed-Field-Gradient NMR*, 1st ed., Springer, Heidelberg, **2014**.
[8] D. C. Ford, D. Dubbeldam, R. Q. Snurr, V. Künzel, M. Wehring, F. Stallmach, J. Kärger, U. Müller, *J. Phys. Chem. Lett.* **2012**, *3*, 930 – 933.
[9] F. Stallmach, S. Gröger, V. Künzel, J. Kärger, O. M. Yaghi, M. Hesse, U. Müller, *Angew. Chem. Int. Ed.* **2006**, *45*, 2123 – 2126; *Angew. Chem.* **2006**, *118*, 2177 – 2181.
[10] M. Wehring, J. Gascon, D. Dubbeldam, F. Kapteijn, R. Q. Snurr, F. Stallmach, *J. Phys. Chem. C* **2010**, *114*, 10527 – 10534.
[11] S. Hertel, M. Wehring, S. Amirjalayer, M. Gratz, J. Lincke, H. Krautscheid, R. Schmid, F. Stallmach, *Eur. Phys. J. Appl. Phys.* **2011**, *55*, 20702 – 20712.
[12] R. Valiullin, *Diffusion NMR of Confined Systems*, 1st ed., RSC, Cambridge, **2016**.
[13] E. M. Forman, M. A. Trujillo, K. J. Ziegler, S. A. Bradley, H. Wang, S. Prabhakar, S. Vasenkov, *Microporous Mesoporous Mater.* **2016**, *229*, 117 – 123.
[14] B. Coasne, *New J. Chem.* **2016**, *40*, 4078 – 4094.
[15] A. Galarneau, F. Guenneau, A. Gedeon, D. Mereib, J. Rodriguez, F. Fajula, B. Coasne, *J. Phys. Chem. C* **2016**, *120*, 1562 – 1569.
[16] M. Gratz, M. Wehring, P. Galvosas, F. Stallmach, *Microporous Mesoporous Mater.* **2009**, *125*, 30 – 34.
[17] P. Galvosas, P. T. Callaghan, *C. R. Phys.* **2010**, *11*, 172 – 180.
[18] S. Couck, J. F. M. Denayer, G. V. Baron, T. Rémy, J. Gascon, F. Kapteijn, *J. Am. Chem. Soc.* **2009**, *131*, 6326 – 6327.
[19] E. Stavitski, E. A. Pidko, S. Couck, T. Remy, E. J. M. Hensen, B. M. Weckhuysen, J. Denayer, J. Gascon, F. Kapteijn, *Langmuir* **2011**, *27*, 3970 – 3976.
[20] Z. Antonio, R. A. Perelta, P. A. Bayliss, R. Howie, M. Sánchez-Serratos, P. Carmona-Monroy, D. Solis-Ibarra, E. González-Zamora, I. A. Ibarra, *RSC Adv.* **2016**, *6*, 9978 – 9983.
[21] J. Kim, W. Y. Kim, W.-S. Ahn, *Fuel* **2012**, *102*, 574 – 579.
[22] P. Serra-Crespo, M. A. van der Veen, E. Gobechiya, K. Houthoufd, Y. Filinchuk, E. A. Kirschhock, J. A. Martens, B. F. Sels, D. E. De Vos, F. Kapteijn, J. Gascon, *J. Am. Chem. Soc.* **2012**, *134*, 8314 – 8317.
[23] Y. An, H. Li, Y. Liu, B. Huang, Q. Sun, Y. Dai, X. Qin, X. Zhang, *J. Solid State Chem.* **2016**, *233*, 194 – 198.
[24] J. Gascon, U. Aktay, M. D. Hernandez-Alonso, G. P. M. van Klink, F. Kapteijn, *J. Catal.* **2009**, *261*, 75 – 87.
[25] X. Cheng, A. Zhang, K. Hou, M. Liu, Y. Wang, C. Song, G. Zhang, X. Guo, *Dalton Trans.* **2013**, *42*, 13698 – 13705.
[26] J. M. Chin, E. Y. Chen, A. G. Menon, H. Y. Tan, A. T. S. Hor, M. K. Schreyer, J. Xu, *CrystEngComm* **2013**, *15*, 654 – 657.
[27] J. Kärger, *Ann. d. Phys.* **1971**, *482*, 107 – 109.
[28] J. Kärger, W. Heink, *J. Magn. Reson.* **1983**, *51*, 1 – 7.
[29] J. Kärger, *AIChe J.* **1982**, *28*, 417 – 423.
[30] J. J. Chen, J. A. Mason, E. D. Bloch, D. Gygi, J. R. Long, J. A. Reimer, *Microporous Mesoporous Mater.* **2015**, *205*, 65 – 69.
[31] Z. R. Hinedi, A. C. Chang, M. A. Anderson, D. B. Borchardt, *Water Resour. Res.* **1997**, *33*, 2697 – 2704.
[32] S. Torquato, M. Avellaneda, *J. Chem. Phys.* **1991**, *95*, 6477 – 6489.
[33] P. Mitra, P. Sen, *Phys. Rev.* **1992**, *45*, 143 – 156.
[34] J. Crank, *The Mathematics of Diffusion*, 1st ed., Oxford, Clarendon Press, **1975**.
[35] J. Kärger, *Adsorption* **2003**, *9*, 29 – 35.
[36] Z. Adem, F. Guennaeu, M. A. Springuel-Huet, A. Gedeon, *Microporous Mesoporous Mater.* **2008**, *114*, 337 – 342.
[37] T. Titze, A. Lauerer, L. Heinke, C. Chmelik, N. E. R. Zimmermann, F. J. Keil, D. M. Ruthven, J. Kärger, *Angew. Chem. Int. Ed.* **2015**, *54*, 14580 – 14583; *Angew. Chem.* **2015**, *127*, 14788 – 14792.
[38] S. Vasenkov, J. Kärger, *Microporous Mesoporous Mater.* **2002**, *55*, 139 – 145.
[39] H. Takaba, A. Yamamoto, K. Hayamizu, S. Nakao, *J. Phys. Chem. B* **2005**, *109*, 13871 – 13876.
[40] A. Feldhoff, J. Caro, H. Jobic, C. B. Krause, P. Galvosas, J. Kärger, *ChemPhysChem* **2009**, *10*, 2429 – 2433.

[41] *Fractals and Disordered Systems*, 2nd ed. (Eds.: A. Bunde, S. Havlin), Springer, Heidelberg, **1996**.
[42] D. Kondrashova, A. Lauerer, D. Mehlhorn, H. Jobic, A. Feldhoff, M. Thommes, D. Chakraborty, C. Gommes, J. Zecevic, P. de Jongh, A. Bunde, J. Kärger, R. Valiullin, *Sci. Rep.* **2017**, *7*, 40207.
[43] M. Holz, S. R. Heil, A. Sacco, *Phys. Chem. Chem. Phys.* **2000**, *2*, 4740 – 4742.
[44] M. J. O'Neil, Royal Society of Chemistry (GB), *The Merck Index—An Encyclopedia of Chemicals, Drugs, and Biologicals*, 15th rev. ed., RSC, Cambridge, **2013**.
[45] C. Jackson, G. McKenna, *J. Chem. Phys.* **1990**, *93*, 9002 – 9011.

Manuscript received: June 6, 2017
Accepted manuscript online: July 19, 2017
Version of record online: August 28, 2017